https://doi.org/10.5194/bg-2020-385
Preprint. Discussion started: 10 November 2020

Biogeosciences Discussions
Open Access
EGU

Variability of North Atlantic CO_2 fluxes for the 2000–2017 period

Zhaohui Chen[1], Parvadha Suntharalingam[1], Andrew J. Watson[2], Ute Schuster[2], Jiang Zhu[3], and Ning Zeng[4]

[1]School of Environmental Sciences, University of East Anglia, Norwich, NR4 7TJ, UK.
[2]College of Life and Environmental Sciences, University of Exeter, Exeter, EX4 4RJ, UK.
[3]International Center for Climate and Environment Sciences, Institute of Atmospheric Physics, Chinese Academy of Science, Beijing,10029, China.
[4]Department of Atmospheric and Oceanic Science, and Earth System Science Interdisciplinary Center, University of Maryland, College Park, Maryland, 20742, USA

Correspondence to: Zhaohui Chen (Zhaohui.chen@uea.ac.uk)

Abstract. We present new estimates of the regional North Atlantic (15°N−80°N) CO_2 flux for the 2000−2017 period using atmospheric CO_2 measurements from the NOAA long term surface site network in combination with an atmospheric data assimilation system (GEOSChem−LETKF). We also assess the sensitivity of flux estimates to the representation of the prior ocean flux distribution and to the associated specification of prior flux uncertainty, including a specification that is dependent on the agreement among the multiple representations of the prior ocean flux. Long term average flux estimates for the 2000−2017 period are -0.26±0.04 PgC y^{-1} for the subtropical basin (15°N–50°N), and -0.25±0.04 PgC y^{-1} for the subpolar region (50°N–80°N, west of 20°E),. Our basin−scale estimates of the standard deviation of interannual variability (IAV) are 0.037±0.006 PgC y^{-1} and 0.025±0.009 PgC y^{-1} for subtropical and subpolar regions respectively. We find a statistically significant trend in carbon uptake for the subtropical North Atlantic of -0.062±0.009 PgC y^{-1} $decade^{-1}$ over this period.

1 Introduction

The ocean plays a key role in the global carbon budget, accounting for 2.5±0.6 PgC y^{-1} (approximately 26%) of the uptake of global fossil emissions during the last decade (period 2009-2018) (Friedlingstein et al., 2019). The North Atlantic ocean has been identified a region of significant net oceanic CO_2 uptake in a range of recent analyses (Schuster et al., 2013, Landschützer et al., 2013, Lebehot et al., 2019), and also the location of the largest Northern Hemisphere uptake of anthropogenic CO_2 in recent decades (Gruber et al., 2019, Khatiwala et al., 2013, Sabine et al., 2004). Recent estimates of net air-sea CO_2 fluxes derived from sea surface partial pressure CO_2 measurements (pCO_2) indicate net annual uptake for the North Atlantic of -0.47 ±0.08 PgC y^{-1} for the 1990−2009 period (Schuster et al., 2013, equivalent to about 20% of global ocean CO_2 uptake). Regionally aggregated air-sea CO_2 fluxes over the North Atlantic basin also display significant variability on interannual (Watson et al., 2009) and decadal timescales (Landschützer et al., 2016, 2019). Based on analyses of surface pCO_2 measurements, variations in regional pCO_2 trends were observed in the subtropical and subpolar regions, potentially associated with large−scale climate oscillations such as the North Atlantic Oscillation and the Atlantic Multi−decadal Variation (McKinley et al., 2011, Landschützer et al., 2019, Macovei et al., 2020). Devries et al. (2019) estimated a negative trend in

https://doi.org/10.5194/bg-2020-385
Preprint. Discussion started: 10 November 2020

Biogeosciences Discussions Open Access EGU

North Atlantic CO_2 uptake based on analysis of pCO_2-based estimates and ocean models for the 2000−2009 period. In addition, Lebehot et al. (2019) found distinct differences between trends in surface ocean CO_2 fugacity (fCO_2) derived from observation-based surface mapping methods and those from the CMIP5 Earth System models.

These recent analyses of North Atlantic air-sea CO_2 fluxes have primarily been based on 'bottom−up' methods of varying complexity which use interpolated surface ocean pCO_2 distributions (derived from in-situ pCO_2 measurements) in combination with parameterizations of air−sea gas exchange (e.g., Landschützer et al., 2013; Rödenbeck et al., 2015; Takahashi et al., 2002; Takahashi et al., 2009). Estimates of air−sea CO_2 fluxes have also been derived by alternative methods such as global ocean biogeochemical models (e.g., Buitenhuis et al.,2013; Law et al., 2017), and 'top−down' methods which involve the application of inverse analyses or data assimilation methods to atmospheric and oceanic CO_2 measurements (e.g., Gruber et al., 2009, Mikaloff−Fletcher et al., 2006, Gurney et al., 2003, Peylin et al., 2013).

Atmospheric CO_2 inversions estimate surface CO_2 fluxes by using information on observed gradients in atmospheric CO_2 together with atmospheric transport constraints (typically from 3 D atmospheric models) and prior information on surface CO_2 flux distributions (Rödenbeck et al., 2003; van der Laan−Luijkx et al., 2017; Peters et al., 2005; Peylin et al., 2013; Chevallier et al., 2014; Gaubert et al., 2019). Previous studies have noted some discrepancies between estimates of regional ocean fluxes from the different methods. For example, Peylin et al. (2013) noted the limited constraints provided by atmospheric CO_2 measurements on land−ocean carbon flux partitioning for some regions, and noted the potential for "flux leakage" between land and ocean flux estimates (e.g., the northern ocean fluxes). Previous studies also found that estimates of carbon fluxes from the atmospheric inverse method are sensitive to the specification of the prior flux distribution and its associated uncertainty distribution (Carouge et al., 2010; Chatterjee et al., 2013; Peylin et al., 2013); While there have been recent studies evaluating the sensitivity of land−based carbon flux estimates to specification of the prior flux and its uncertainty, the variation of regional ocean fluxes has been far less examined by previous inverse studies.

Previous inverse estimates of ocean CO_2 fluxes have predominantly relied on the climatological ocean to atmosphere CO_2 flux distribution of Takahashi et al. (2009) for use as the a priori flux estimate (e.g., Nassar et al., 2011; Feng et al., 2009, 2016; Deng et al., 2016). These analyses often use different methods to specify the level of flux uncertainty assigned to the ocean prior fluxes. For example, the inverse analyses of Feng et al. (2016) and Deng et al. (2016) use prior flux uncertainty levels of 0.6 PgC y^{-1} (equivalent to 44% of the ocean flux total) , i.e., a level of uncertainty twice as large as the uncertainty in Nassar et al. (2011).

Here we present a new long term estimate of North Atlantic air−sea CO_2 fluxes for recent decades (period 2000−2017) using atmospheric inverse methods. We use the carbon cycle data assimilation system GEOSChem−LETKF (GCL) which combines the global atmospheric CO_2 transport model GEOS−Chem (Nassar et al., 2010) with the Localized Ensemble Transform Kalman Filter (LETKF) data assimilation system (Hunt et al., 2007; Miyoshi et al., 2007; Liu et al., 2019). An additional focus of our analysis is to evaluate the sensitivity of flux estimates to alternative a priori flux distributions and uncertainty specifications for oceanic CO_2 fluxes. To our knowledge these influences on North Atlantic flux estimates have not been assessed previously.

https://doi.org/10.5194/bg-2020-385
Preprint. Discussion started: 10 November 2020

We investigate the sensitivity of the derived posterior flux estimates to three different representations of the ocean prior flux distribution and investigate an alternative method to characterize prior ocean flux uncertainty based on the ensemble spread of the multiple prior ocean fluxes. We derive North Atlantic CO_2 flux estimates for the 2000–2017 period and compare their characteristics with previous relevant studies.

2 Materials and Methods

2.1 Overview

Our analysis employs the Localised Ensemble Kalman Filter (section 2.2) together with the global GEOS-Chem atmospheric chemistry transport model (section 2.3) and atmospheric CO_2 observations from the NOAA–ESRL network of surface sites (section 2.4). Section 2.5 describes the specification of flux uncertainty based on multiple representations of prior ocean fluxes (spread–based uncertainty). Section 2.6 presents sensitivity analyses assessing different prior flux representations and flux uncertainties defined from three different schemes (i.e., percentage–based uncertainty specifications (60%, 120%), and the spread–based uncertainty scheme). Further details on the methods, model, observations and uncertainty calculations are presented in the sections below and in the Appendix.

2.2 Localized Ensemble Transform Kalman Filter (LETKF)

The LETKF is a data assimilation system which provides an estimate given a prior (or "background") estimate of the current state based on past and current data (in this case, the atmospheric CO_2 mole fraction observations). The general framework of the LETKF is described in Hunt et al. (2007); it has been adapted by Miyoshi et al. (2007) to provide gridscale localized analysis of flux estimates. The LETKF system has been used to estimate CO_2 fluxes in a range of previous studies (e.g, Kang et al., 2012; Liu et al., 2016, 2019).

The LETKF provides iterative estimates of the time evolution of the system state, x, (here representing the gridscale surface carbon fluxes). Each step involves a forecast stage (based on a physical model of the system evolution) and a state estimation stage (the 'analysis' step), which combines system observations, y, together with the background forecast, x^b, to derive the improved state estimate. The observation operator H provides the mapping from the state space to the observation space; in this study H is provided by the GEOS–Chem atmospheric model (section 2.3). Further details on the LETKF and the governing equations for flux estimation are provided in the Appendix A1.

In this analysis, the LETKF is used to derive gridscale fluxes for the period 2000–2017. The gridded fluxes are updated sequentially on weekly timescale by assimilation of the atmospheric CO_2 observations from a network of surface sites (section

https://doi.org/10.5194/bg-2020-385
Preprint. Discussion started: 10 November 2020

2.4). We report a posteriori fluxes on monthly timescales for the 2000–2017 period; the optimized monthly fluxes are derived from four sequential weeks of assimilation cycles.

2.3 The GEOS–Chem atmospheric transport model

The GEOS–Chem atmospheric chemistry transport model has been used in a range of previous investigations into atmospheric CO_2 and applied in conjunction with inverse analyses to estimate surface carbon fluxes (Nassar et al., 2010, 2011; Suntharalingam et al., 2005; Liu et al., 2016). In this analysis we employ GEOSChem v11–01 at a horizontal resolution of 2° latitude by 2.5° longitude, with 47 levels in the vertical. Model transport fields are provided by GEOS-5 assimilated meteorological data from the NASA Global Modeling and Assimilation Office (GMAO, Rienecker et al., 2008). A detailed information of prior fluxes and uncertainties used in this study is given in Section 2.5.

2.4 Atmospheric CO_2 Observations

Atmospheric CO_2 observations used for this study are taken from the NOAA–ESRL GLOBALVIEWplus Observation Package v4.2 (Obspack, Cooperative Global Atmospheric Data Integration Project, 2018). CO_2 measurement records for the period 2000–2017 from 86 surface sites were used in this analysis. Further details on the measurement sites and the site-specific observation uncertainty characteristics are presented in Table A1 of the Appendix. The specification of observational uncertainty associated with incorporation of the atmospheric CO_2 measurements into the LETKF is derived using the methods of Chevallier et al. (2010); we use the standard deviation of measurement variability from detrended and deseasonalized CO_2 time series at each measurement site. The resulting specification of observational uncertainty varies between 0.16 ppm (for stations in and around the Southern Ocean) to over 5 ppm (for stations in continental interiors) (see Appendix Table A1 for more details).

2.5 Specification of Prior CO_2 Fluxes and Associated Flux Uncertainties

A priori CO_2 flux distributions implemented in the GEOS–Chem model for this analysis include fossil fuel emissions taken from Chevallier et al. (2019) (Global Atmospheric Research version 4.3.2, Crippa et al., 2016, scaled globally and annually from Le Quéré et al., 2018), and land biosphere fluxes from the Joint UK Land Environment Simulator (JULES, Clark et al., 2011). We evaluate three separate representations for ocean CO_2 fluxes, namely, Takahashi et al. (2009) (hereinafter Ta), Landschützer et al. (2016) (hereinafter La), and Rödenbeck et al. (2013) (hereinafter Ro).

Since the primary focus of our investigation is to estimate North Atlantic Ocean CO_2 fluxes, we have evaluated in more detail, the impact of different specifications of prior flux uncertainty for ocean fluxes. Specifications of prior flux uncertainty for ocean fluxes include (a) a percentage-based level (U1:60% of prior flux, and U2:120% of prior flux), and (b) gridded flux uncertainties representing the variation or 'spread' of the different ocean flux data products at each location, and based on the standard deviation of the variation among the prior fluxes (U3: spread-based uncertainty; see equation 1). This specification follows previously used methods to characterize uncertainties in ocean flux distributions (e.g., Bopp et al., 2013). For this

https://doi.org/10.5194/bg-2020-385
Preprint. Discussion started: 10 November 2020

latter specification (U3), the gridded prior flux uncertainty, *U(i,j)* (for a gridcell with coordinates *(i,j)*) is specified as the standard deviation of the spread of the different prior flux products. Thus, the uncertainty *U(i,j)* is calculated as:

$$U(i,j) = sqrt(\sum_{k}^{K}\left(f_k(i,j) - \overline{f(i,j)}\right)^2)/(K-1) \quad (1)$$

Here K is the total number of the prior ocean flux products considered, and subscript k refers to an individual flux product. $f_k(i,j)$ represents the gridded monthly flux for each prior ocean flux and $\overline{f(i,j)}$ is the gridded monthly mean across all prior ocean flux products. These prior flux uncertainties are estimated on monthly timescales and also account for interannual variations. The representation of ocean prior flux uncertainty is further discussed in section 3.1.

3 Results and Discussion

Section 3.1 and Table 1 present sensitivity tests conducted for different prior ocean flux distributions and prior ocean flux uncertainty schemes. Section 3.2 presents the estimates of North Atlantic CO_2 ocean fluxes for the 2000–2017 period. We focus on the long term mean values, interannual variability and trends of the GCL estimates of CO_2 ocean fluxes. In section 3.2 we also compare the results from this study with previous estimates of North Atlantic (NA) fluxes.

3.1 Sensitivity tests on specification of prior flux uncertainty

We first assess the sensitivity of derived flux estimates to the specification of prior flux uncertainty; this analysis is conducted for the year 2003. An initial three year model spin−up, starting from January 1st, 2000 was conducted following the CO_2 simulation and methods of Nassar et al. (2010). We evaluate the sensitivity of posterior ocean flux estimates with three different prior ocean uncertainty schemes U1, U2, and U3, described in section 2.5; these are applied in turn for each of the three prior ocean flux distributions (Ta, La and Ro). Figure 1 presents an example distribution of the spread−based prior ocean flux uncertainty U3 (shown as a quarterly average for an example year of 2003). Figure 1 demonstrates that the spread-based uncertainty scheme (U3) provides a looser constraint on prior fluxes (i.e., levels of prior flux uncertainty > 120%) than the U1 and U2 schemes in the subpolar region, and a tighter constraint in the subtropical region (levels < 60%).

https://doi.org/10.5194/bg-2020-385
Preprint. Discussion started: 10 November 2020

Biogeosciences
Discussions
Open Access
EGU

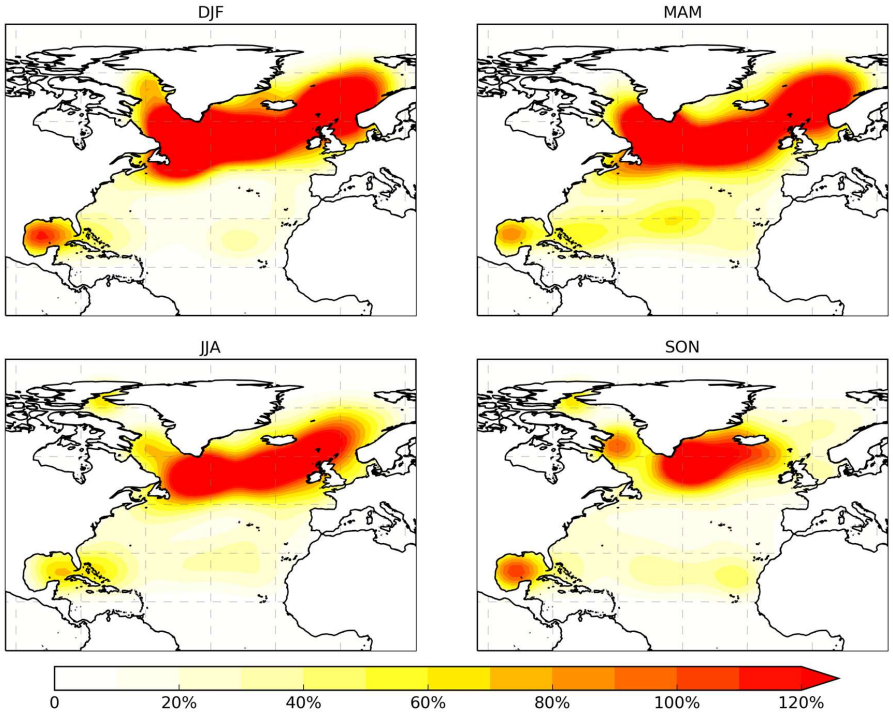

145

Figure 1. Distribution of the spread-based prior ocean flux uncertainty (U3) (annual average for the year 2003). It is represented here as a percentage of the prior ocean flux for ease of comparison with U1 and U2. The percentage shown for each grid-cell is derived from the ratio of spread−based prior ocean uncertainty divided by the prior ocean flux value at that grid cell. DJF represents the monthly average for December, January, February; MAM for March, April, May; JJA for June, July, August; SON for September, October, November.

150

Table 1 summarizes the prior and posterior ocean flux estimates for the global and North Atlantic region (sub-divided into subpolar and subtropical regions) from the respective sensitivity tests. The distribution of prior flux for the subtropical North Atlantic shows closer agreement among the three source representations (Ta, La and Ro), with regional variation of 0.05 PgC y^{-1}, in comparison to a regional variation of ~0.1 PgC y^{-1} for the subpolar region.

155 Under the constraints provided by the atmospheric CO_2 observations all posterior flux estimates for the North Atlantic show increased uptake (Table 1), indicating that all three representations of ocean prior flux underestimate the regional net atmosphere-ocean flux for the 2003 period. Our estimates indicate a larger increase in CO_2 uptake in the subpolar basin (~0.05 PgC y^{-1}, changing from a prior flux range of -0.13 to -0.23 PgC y^{-1} to posterior flux range of -0.19 to -0.28 PgC y^{-1}), in comparison to the smaller magnitude change for the subtropical North Atlantic basin (of ~ 0.02 PgC y^{-1} from -0.17 to -0.22

160 PgC y^{-1} to -0.2 to -0.25 PgC y^{-1})

https://doi.org/10.5194/bg-2020-385
Preprint. Discussion started: 10 November 2020

Table 1. Global and North Atlantic CO_2 flux estimates from the GEOSChem−LETKF(GCL) system for year 2003 (PgC y^{-1}) summarizing sensitivity analyses on the prior ocean flux distribution. Prior flux references are Ta: Takahashi et al. 2009; La: Landschutzer et al. 2017; Ro: Rodenbeck et al. 2013. Prior flux uncertainty specifications are: U1 60%; U2: 120%: U3: spread−based (following methods of section 2.5).

Global Ocean CO_2 Flux (PgC y^{-1})					
Ta	-1.37	La	-1.25	Ro	-2.09
TaU1	-1.63±0.13	LaU1	-1.52±0.13	RoU1	-2.31±0.16
TaU2	-2.05±0.26	LaU2	-1.96±0.26	RoU2	-2.68±0.31
TaU3	-2.24±0.28	LaU3	-2.21±0.28	RoU3	-2.73±0.28
North Atlantic subtropics [15°N-50°N]					
Ta	-0.22	La	-0.18	Ro	-0.17
TaU1	-0.23±0.02	LaU1	-0.19±0.02	RoU1	-0.18±0.02
TaU2	-0.25±0.05	LaU2	-0.21±0.04	RoU2	-0.20±0.04
TaU3	-0.24±0.05	LaU3	-0.20±0.05	RoU3	-0.19±0.05
North Atlantic subpolar [50°N-80°N], west of 20°E					
Ta	-0.23	La	-0.13	Ro	-0.21
TaU1	-0.23±0.05	LaU1	-0.13±0.02	RoU1	-0.22±0.04
TaU2	-0.25±0.1	LaU2	-0.14±0.05	RoU2	-0.23±0.09
TaU3	-0.28±0.11	LaU3	-0.19±0.11	RoU3	-0.26±0.11

We note that the increases in estimated uptake for the North Atlantic basins are relatively smaller (on average in the range 10−20%) than the increased uptake estimated on the global scale (~30−70% changes, see Table 1), indicating that prior flux representations of the North Atlantic are more consistent with the constraints from atmospheric measurements than those for other regions of the global ocean.

Use of the spread−based uncertainty scheme (U3) enables flexibility in specification of the regional magnitude of the prior flux uncertainty, as it allows tighter constraints in regions where alternative prior flux representations are in accord, and looser constraints in regions where prior flux representations differ significantly. For the long term analyses of the remainder of this study we therefore use the U3 flux uncertainty scheme. We will also employ the flux distribution of Landschützer et al. (2016) as the prior flux distribution as it provides interannually varying fluxes over the entire estimation period (2000−2017).

3.2 Multi-year analyses of North Atlantic CO_2 fluxes

In this section we present results of a multi−year analysis (for the period 2000−2017) assessing regional estimates of North Atlantic CO_2 fluxes on annual to decadal timescales. We assess the GCL a posteriori estimates of ocean fluxes using the prior flux specifications outlined in section 2; i.e., La, Ro and Ta. All other prior flux distributions (for fossil emissions, and land biosphere fluxes) are as described in section 2.4. To evaluate the inverse results in this study further, we compare our results

https://doi.org/10.5194/bg-2020-385
Preprint. Discussion started: 10 November 2020

with the estimates from three other inverse systems including CAMS (v18r2, Chevallier et al., 2019), CT (CarbonTracker 2019, Jacobson et al., 2020) and CTE (Carbon Tracker Europe, van der Laan−Luijkx et al., 2017). All data are regridded to 2° latitude × 2.5° longitude to be consistent with the GCL model resolution.

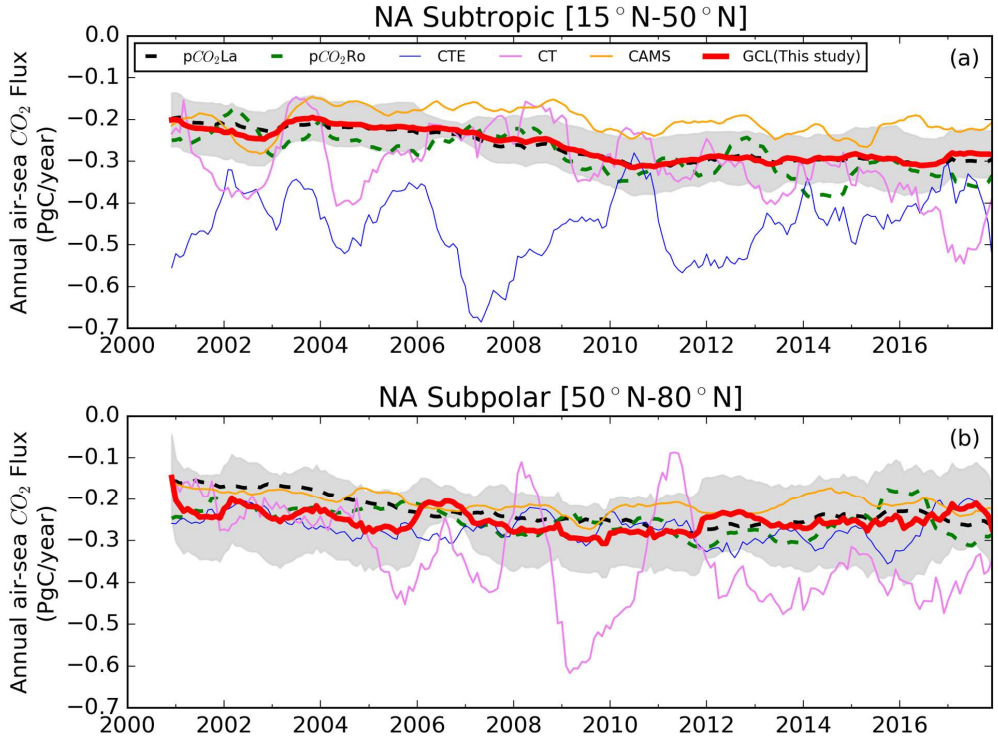

Figure 2. Comparison of annual air−sea CO_2 fluxes for North Atlantic for the 2000−2017 period for: (a) North Atlantic Subtropics; and (b) North Atlantic Subpolar regions. The GCL posterior flux estimate from this study (red) is derived from the prior flux of Landschützer et al., 2016 (pCO_2La: black). The grey shaded area represents the uncertainty estimate on the GCL posterior flux (plotted at a 3 sigma level). Also shown are the flux estimates of (i) Chevallier et al., 2019 (CAMS: yellow); (ii) Jacobson et al., 2020 (CT: CarbonTracker2019: pink); and (iii) van der Laan−Luijkx et al., 2017 (CTE: Carbon Tracker Europe: blue). All time series shown have a 12 month running mean filter applied.

Figure 2 presents the variation of air−sea CO_2 flux for the NA subtropical and subpolar regions for the 2000−2017 period (represented as a 12 month running average), and comparison to estimates from previous studies. For the NA subtropical region, the GCL posterior flux magnitude is similar to that of the prior flux, with a difference of less than 0.02 PgC y^{-1} over the period. Variation among the other inverse flux estimates can reach up to 0.5 PgC y^{-1} (e.g., between CTE and CAMS in 2007). These larger variations primarily result from the different prior ocean fluxes used in the respective inverse studies. This

https://doi.org/10.5194/bg-2020-385
Preprint. Discussion started: 10 November 2020

issue has been previously noted by other studies; e.g., Nassar et al. (2011), note that that the prior ocean flux used in CTE (Jacobson et al., 2007; van der Laan−Luijkx et al., 2017) provides approximately 85% more carbon uptake (on a global basis) than the ocean flux estimates of Takahashi et al. (2009).

For the NA subpolar region, the GCL posterior flux estimate deviates more from the prior flux estimate (e.g., showing differences of up to 0.09 PgC y^{-1}), especially in the early decade of the analysis (2000−2010). The majority of flux estimates for the NA subpolar region are in closer accord (Fig. 2b) with differences of less than 0.2 PgC y^{-1} (the CT estimate is an exception indicating variations of greater than 0.3 PgC y^{-1} from the other estimates). The long term mean, IAV and trends of these estimates are discussed in the following subsections.

3.2.1 Long term mean

Figure 3 provides a comparison of the following GCL flux estimates and associated characterstics for the North Atlantic subtropical and subpolar regions for the period 2000−2017: (i) the long term mean of air−sea CO_2 flux estimates (The underlying data are tabulated in Table 2); (ii) the amplitude of estimated interannual variability (IAV) of fluxes (Table 3); and (iii) the long term trends (Table 4). The IAV is calculated following methods of Rödenbeck et al. (2015) (i.e., derived from the standard deviation of the residuals of a 12 month running mean over the CO_2 flux time series).

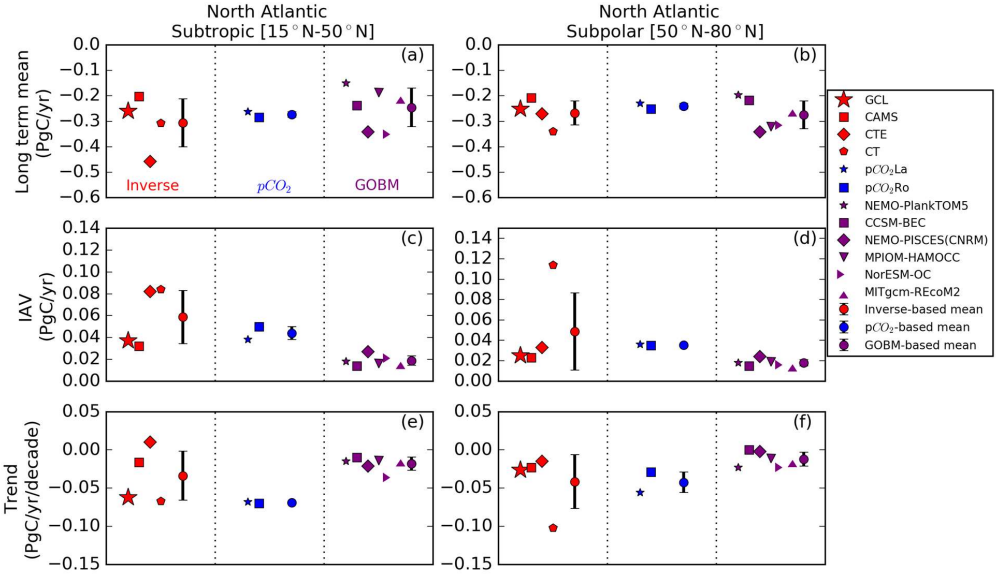

Figure 3. Comparison of CO_2 ocean flux metrics for the 2000−2017 period for North Atlantic subtropics (left panels) and subpolar regions (right panels). Metrics shown are the long term mean (panels (a) and (b)); interannual variability (IAV) (panels (c) and (d)); and long term trend (panels (e) and (f)). The GCL estimates (red stars) are shown in comparison to other atmospheric inverse analyses (red symbols),

https://doi.org/10.5194/bg-2020-385
Preprint. Discussion started: 10 November 2020

surface ocean pCO_2 products (blue) and global ocean biogeochemistry models (GOBMs, purple). Also shown are the estimated means from each sub-group of analyses (circle symbols) with associated uncertainty (1 standard deviation).

Table 2. Summary metrics of GEOSChem−LETKF North Atlantic (NA) CO_2 flux estimates, and comparison with independent estimates (from atmospheric inverse analyses, surface pCO_2 mappings, and Global Ocean Biogeochemistry models (GOBMs)) for the period 2000−2017. Listed are estimates for the long term mean. The metrics listed in this table are plotted in Fig. 3.

Long term mean (PgC y^{-1})		
NA Subtropics	NA Subpolar	
Atmospheric inversions		
-0.26±0.04	*-0.25±0.04*	*This study (GCL)*[a]
-0.203	-0.208	CAMS (Chevallier et al. 2019)
-0.457	-0.270	CTE (van der Laan−Luijkx et al. 2017)
-0.307	-0.34	CT (Jacobson et al. 2020)
-0.30±0.11	-0.26±0.05	Mean of all atmospheric inverse studies[b]
Surface ocean pCO_2-based flux products		
-0.263	-0.23	pCO_2La (Landschutzer et al. 2016)
-0.284	-0.252	pCO_2Ro (Rodenbeck et al. 2013)
-0.27±0.01	-0.24±0.01	Mean of all pCO_2-based representations[b]
Global ocean biogeochemistry models		
-0.150	-0.197	NEMO-PlankTOM5 (Buitenhuis et al. 2010)
-0.238	-0.217	CCSM-BEC (Doney et al. 2009)
-0.342	-0.341	NEMO-PISCES (CNRM) (Séférian et al. 2013)
-0.188	-0.321	MPIOM-HAMOCC (Ilyina et al. 2013)
-0.351	-0.316	NorESM-OC (Schwinger et al. 2016)
-0.205	-0.256	MITgcm-REcoM2 (Hauck et al. 2016)
-0.24±0.07	-0.27±0.05	Mean of GOBM studies[b]

We also present in Fig. 3 the equivalent estimates from other independent assessments, including (i) other atmospheric inverse analyses, (ii) surface ocean pCO_2−based analyses, and (iii) analyses from global ocean biogeochemistry models (GOBMs, Buitenhuis et al., 2010; Doney et al., 2009; Séférian et al., 2013; Ilyina et al., 2013; Schwinger et al., 2016; Hauck et al., 2016).

For the North Atlantic subtropical region, the long term mean of the GCL posterior flux estimate is -0.26±0.04 PgC y^{-1}. This is consistent with the observationally based "best" estimate of Schuster et al. (2013) for the period 1990-2009. Figure 3 (and Table 2) also indicate generally good agreement between the GCL estimate for North Atlantic subtropical region fluxes and

https://doi.org/10.5194/bg-2020-385
Preprint. Discussion started: 10 November 2020

estimates from surface pCO_2−based methods and GOBMs. The GCL inverse estimate is also consistent with 2 of the other 3 inverse flux estimates considered, with only the flux estimate from CTE (van der Laan−Luijkx et al., 2017) significantly different with an uptake level greater than 0.4 PgC y^{-1}. For the North Atlantic subpolar region, the GCL estimate of the long term mean uptake is -0.25±0.04 PgC y^{-1} (Table 2), which is slightly larger than that of the prior flux (-0.23 PgC y^{-1}) and the estimate of -0.21 PgC y^{-1} from Schuster et al. (2013). The ensemble mean from each group (atmospheric inversions, pCO_2−based and GOBMs) agree well and range from -0.24 PgC y^{-1} to -0.27 PgC y^{-1}.

3.2.2 Interannual variability

The standard deviation of IAV derived from the GCL is 0.037±0.006 PgC y^{-1} for the NA subtropics and 0.025±0.009 PgC y^{-1} for the NA subpolar region (Fig. 3, Table 3). The IAV estimates for the NA subtropics from the different analyses display a large range of values (0.019 to 0.059 PgC y^{-1}). The standard deviation of IAV derived from the GCL (~0.037 PgC y^{-1}) is similar to that of the prior and of the surface ocean pCO_2−based estimates but larger than those of the GOBMs (~0.019 PgC y^{-1}). The largest IAV estimates (mean value of 0.059±0.024 PgC y^{-1}) are associated with the atmospheric inversions, and influenced by the CarbonTracker analyses (e.g., CTE and CT indicate larger IAV magnitudes for this period of ~0.08 PgC y^{-1}). Potential causes of the differences between the GCL and CAMS IAV estimates and those of the CarbonTracker estimates are the different prior ocean fluxes employed by the different inverse analyses, and the relative weighting assigned to the influence of atmospheric CO_2 observations (Jacobson et al., 2019). The GCL and CAMS estimates use the prior flux of Landschützer et al. (2016) and the CarbonTracker inversions use the prior flux of Jacobson et al. (2007).

The GCL estimate of IAV for the North Atlantic subpolar region (~0.025 PgC y^{-1}) is closer in magnitude to the majority of other analyses, which range between 0.015 and 0.036 PgC y^{-1} (the exception being the CT inverse estimate with the largest IAV of 0.114 PgC y^{-1}). For this region the IAV estimates from atmospheric inverse analyses display the greatest variation, influenced by the high estimate from the CT analysis.

https://doi.org/10.5194/bg-2020-385
Preprint. Discussion started: 10 November 2020

Table 3. Summary metrics of GEOSChem−LETKF North Atlantic (NA) CO_2 flux estimates, and comparison with independent estimates (from atmospheric inverse analyses, surface pCO_2 mappings, and Global Ocean Biogeochemistry models (GOBMs)) for the period 2000−2017. Listed are estimates for the trend of the regional fluxes over the period. The metrics listed in this table are plotted in Fig. 3.

Interannual Variability (IAV) (PgC y^{-1})		
NA Subtropics	NA Subpolar	
Atmospheric inversions		
0.037±0.006	*0.025±0.009*	*This study (GCL)*[c]
0.032	0.023	CAMS (Chevallier et al. 2019)
0.082	0.033	CTE (van der Laan−Luijkx et al. 2017)
0.084	0.114	CT (Jacobson et al. 2020)
0.059±0.024	0.049±0.038	Mean of all Atmospheric inverse studies[b]
Surface ocean pCO_2−based flux products		
0.038	0.036	pCO_2La (Landschutzer et al. 2016)
0.050	0.035	pCO_2Ro (Rodenbeck et al. 2013)
0.044±0.006	0.036±0.001	Mean of all pCO_2-based representations[b]
Global ocean biogeochemistry models		
0.018	0.018	NEMO−PlankTOM5 (Buitenhuis et al. 2010)
0.014	0.015	CCSM-BEC (Doney et al. 2009)
0.027	0.024	NEMO-PISCES (CNRM) (Séférian et al. 2013)
0.016	0.019	MPIOM-HAMOCC (Ilyina et al. 2013)
0.021	0.016	NorESM-OC (Schwinger et al. 2016)
0.017	0.016	MITgcm-REcoM2 (Hauck et al. 2016)
0.019±0.004	0.018±0.003	Mean of GOBM studies[b]

3.2.3 Estimated Trends of North Atlantic CO_2 Fluxes

Our GCL analyses indicate a statistically significant trend of -0.062±0.009 PgC y^{-1} $decade^{-1}$. i.e., increasing CO_2 uptake in the North Atlantic subtropical basin for the 2000−2017 period (significant at the 95% level with Ordinary Least Squares (OLS, Montgomery et al., 2012) method). This estimated trend is of larger magnitude than those estimated from the GOBMs air-sea fluxes (Fig. 3, Table 4), and of similar magnitude to the trends derived for the surface ocean pCO_2−based estimates.

https://doi.org/10.5194/bg-2020-385
Preprint. Discussion started: 10 November 2020

In the North Atlantic subpolar region, GCL estimate of the trend in regional CO_2 uptake of -0.026±0.015 PgC y^{-1} $decade^{-1}$ is larger than the mean estimate from GOBM analyses, and similar to the majority of other atmospheric inverse analyses (apart from the CT inversion which displays a large estimated trend of -0.1 PgC y^{-1} $decade^{-1}$). However, we also note that our derived estimate of trend for this region is not significant at the 95% confidence level.

Table 4. Summary metrics of GEOSChem-LETKF North Atlantic (NA) CO_2 flux estimates, and comparison with independent estimates (from atmospheric inverse analyses, surface pCO_2 mappings, and Global Ocean Biogeochemistry models (GOBMs)) for the period 2000−2017. Listed are estimates for the trend of the regional fluxes over the period. The metrics listed in this table are plotted in Fig. 3 of the main study.

Trend (PgC y^{-1} $decade^{-1}$)		
NA Subtropics	NA Subpolar	
Atmospheric inversions		
-0.062±0.009 (S[d])	*-0.026±0.015*	*This study (GCL)[e]*
-0.016	-0.023	CAMS (Chevallier et al. 2019)
0.010	0.015	CTE (van der Laan−Luijkx et al. 2017)
-0.067	-0.102	CT (Jacobson et al. 2020)
-0.034±0.032	-0.041±0.035	Mean of all Atmospheric inverse studies[b]
Surface ocean pCO_2-based flux products		
-0.068	-0.056	pCO_2La (Landschutzer et al. 2016)
-0.070	-0.029	pCO_2Ro (Rodenbeck et al. 2013)
-0.069±0.001	-0.043±0.013	Mean of all pCO_2-based representations[b]
Global ocean biogeochemistry models		
-0.015	-0.023	NEMO-PlankTOM5 (Buitenhuis et al. 2010)
-0.010	0.000	CCSM-BEC (Doney et al. 2009)
-0.021	-0.002	NEMO-PISCES (CNRM) (Séférian et al. 2013)
-0.014	-0.011	MPIOM-HAMOCC (Ilyina et al. 2013)
-0.036	-0.023	NorESM-OC (Schwinger et al. 2016)
-0.013	-0.014	MITgcm-REcoM2 (Hauck et al. 2016)
-0.018±0.009	-0.018±0.009	Mean of GOBM studies[b]

[a] The uncertainty of long term mean estimate from the GCL (this study) is calculated as the standard deviation of the annual flux estimates over the (2000−2017) period.

[b] The uncertainty of atmospheric-inverse-based mean, pCO_2-based mean and GOBM-based mean is calculated as the standard deviation of products for each method.

https://doi.org/10.5194/bg-2020-385
Preprint. Discussion started: 10 November 2020

[c] The uncertainty of the estimated IAV from the GCL (this study) is calculated as the standard deviation of the ensemble posterior fluxes

[d] The symbol (S) indicates that the calculated trend is statistically significant (at the 95% confidence interval).

[e] The uncertainty of the fitted trend from the GCL estimates is reported as 1 standard deviation of the OLS fitted slope (Montgomery et al. 2012).

4 Summary

Our GCL estimates of CO_2 uptake in the North Atlantic for the 2000−2017 period are -0.26±0.04 PgC y^{-1} for the NA subtropics and -0.25±0.04 PgC y^{-1} for NA subpolar region. The GCL estimates of interannual variability in air−sea CO_2 fluxes are 0.037±0.006 PgC y^{-1} (NA subtropics) and 0.025±0.009 PgC y^{-1} (NA subpolar). Our GCL estimates also indicate a statistically significant trend of increasing CO_2 uptake for the NA subtropics (estimated trend of -0.062±0.009 PgC y^{-1} $decade^{-1}$).

Our GCL estimates of long term mean CO_2 uptake for the 2000−2017 period for both NA subtropics and subpolar regions lie between the estimates from other inverse analyses (e.g., Chevallier et al., 2019 (lower) and the CarbonTracker derived analyses of Jacobson et al., 2020 (higher)); primary causes are the different prior flux representations used in the CarbonTracker analyses. Our GCL estimates of long term North Atlantic CO_2 uptake are similar in magnitude to long term ensemble mean estimates from surface−ocean pCO_2 methods and GOBMs (Fig. 3). The magnitude of IAV derived from the GCL is similar to that of the surface ocean pCO_2-based estimates but larger than those of the GOBMs for both NA regions.

In this study we have also evaluated a comparison of alternative specifications of the prior flux uncertainty (section 3.2), and present long term flux estimates derived using a spread−based flux uncertainty scheme. This scheme enables representation of the variability among alternative prior ocean CO_2 flux representations and ascribes higher levels of uncertainty to regions with larger discrepancies among prior flux representations; it is therefore preferable to the fixed prior flux uncertainty levels commonly used in inverse analyses. Incorporation of additional prior flux representations of ocean CO_2 (e.g., Roedenbeck et al., 2015) will improve the contribution of this scheme.

Air−sea CO_2 flux estimates and associated metrics derived from our GCL analyses are generally more robust for the NA subtropics than for the NA subpolar region. Limiting factors affecting estimates for the NA subpolar region include higher levels of uncertainty associated with (a) specification of prior fluxes (Fig. 1), and (b) the observational uncertainty at the atmospheric measurement CO_2 sites in these high northern latitudes (Table A1). The number of regional atmospheric CO_2 measurement sites available to constrain NA subpolar fluxes are also relatively few. Improved ocean CO_2 flux estimates for this North Atlantic region will be obtained by provision of additional high accuracy marine boundary layer CO_2 measurements for the region from fixed surface sites and from ships and buoys (Wanninkhof et al., 2019).

https://doi.org/10.5194/bg-2020-385
Preprint. Discussion started: 10 November 2020

Appendix A: The Local Ensemble Transform Kalman Filter (LETKF) system

Here we briefly describe the LETKF system used for estimation of surface CO_2 fluxes. The methodology follows that of Hunt et al. (2007) and Miyoshi et al. (2007), and additional detail is provided in these publications. The LETKF has been previously used in meteorological forecasting, and more recently in atmospheric CO_2 data assimilation (e.g., Liu et al. 2019, 2016; Kang et al. 2012). The LETKF provides iterative estimates of the time evolution of the system state, *x,* (here representing the gridscale surface carbon fluxes, of dimension *m*). Each step involves a forecast stage (based on a physical model of the system evolution) and a state estimation stage (the 'analysis' step), which combines system observations, *y* (of dimension *n*), together with the background forecast, x^b, to derive the improved state estimate. The observation operator *H* provides the mapping from the state space to the observation space; in this study *H* is provided by the GEOSChem atmospheric model. In the analysis step, the surface carbon flux estimates are obtained by minimization of a cost function (Equation S1) which accounts for deviations of the system state *x*, from the background forecast, x^b, and for the mismatch between observations (*y*) and their modeled representations (*Hx*) :

$$J(x) = (x - x^b)^T B^{-1}(x - x^b) + (y - Hx)^T R^{-1}(y - Hx) \quad \text{(A1)}$$

B represents the background flux covariance matrix, and *R* represents the observation covariance matrix.

In the LETKF system, an ensemble of model simulations is used to calculate the sample mean and covariance of the system state; thus, the background state x^b is given by $(x^{b(i)}: i = 1.2, \dots k)$ for k ensemble members. The sample mean $\bar{x}^b$ and covariance P^b of the background state vector given by :

$$\bar{x}^b = k^{-1} \sum_{i=1}^{k} x^{b(i)} \quad \text{(A2)}$$

$$P^b = (k-1)^{-1} \sum_{i=1}^{k} \left(x^{b(i)} - \bar{x}^b\right)\left(x^{b(i)} - \bar{x}^b\right)^T \quad \text{(A3)}$$

$$= (k-1)^{-1} X^b (X^b)^T$$

X^b is an $m \times k$ matrix whose *i*th column is $x^{b(i)} - \bar{x}^b$. P^b is the background state covariance matrix ($m \times m$).

Similarly the analysis state is represented by the ensemble $(x^{a(i)}: i = 1,2, \dots k)$ with its sample mean and covariance given by:

$$\bar{x}^a = k^{-1} \sum_{i=1}^{k} x^{a(i)} \quad \text{(A4)}$$

$$P^a = (k-1)^{-1} \sum_{i=1}^{k} \left(x^{a(i)} - \bar{x}^a\right)\left(x^{a(i)} - \bar{x}^a\right)^T \quad \text{(A5)}$$

$$= (k-1)^{-1} X^a (X^a)^T$$

where X^a is the $m \times k$ matrix whose ith column is $x^{a(i)} - \bar{x}^a$.

https://doi.org/10.5194/bg-2020-385
Preprint. Discussion started: 10 November 2020

The analysis state and covariance $\bar{x}^a$ and P^a are updated based on the background information $\bar{x}^b$ and observations y through the following equations:

$$\bar{x}^a = \bar{x}^b + P^a H^T R^{-1}(y - Hx^b) \quad \text{(A6)}$$

$$P^a = (I + P^b H^T R^{-1} H)^{-1} P^b \quad \text{(A7)}$$

The ensemble $y^{b(i)}$ of background observation vectors is defined by:

$$y^{b(i)} = H(x^{b(i)}) \quad \text{(A8)}$$

$$H(\bar{x}^b + X^b w) \approx \bar{y}^b + Y^b w \quad \text{(A9)}$$

where Y^b is the $n \times k$ matrix whose ith column is $(y^{b(i)} - \bar{y}^b)$, and w is a Gaussian random vector with mean $\bar{w}^b = 0$ and covariance $\tilde{P}^b = (k-1)^{-1} I$ .Then the analogues of analysis equations (6) and (7) are:

$$\bar{w}^a = \tilde{P}^a (Y^b)^T R^{-1}(y - \bar{y}^b) \quad \text{(A10)}$$

$$\tilde{P}^a = [(k-1)I + (Y^b)^T R^{-1} Y^b]^{-1} \quad \text{(A11)}$$

Following Hunt et al. (2007) and Miyoshi et al. (2007) (refer to these publications for the complete LETKF derivation) the overall analysis equation is:

$$x = \bar{x}^b + X^b [\tilde{P}^a (Y^b)^T R^{-1}(y - \bar{y}^b) + [(k-1)\tilde{P}^a]^{1/2}] \quad \text{(A12)}$$

The LETKF allows flexibility in the choice of observations to be assimilated at each grid point, based on the distance (r) of the observations from the gridpoint. The localization weighting function $f(r)$ is given by:

$$f(r) = \exp\left(-\frac{r^2}{2L^2}\right) \quad \text{(A13)}$$

where L is an observation localization length which can be predefined to determine the outer boundary of the influence of the observations; i.e., the localization weighting function drops to zero at a value of

$$r = 2.\sqrt{\frac{10}{3}L} \quad \text{(A14)}$$

The observation localization is realized by multiplying the inverse of the localization function $f(r)$ with the observational error covariance R.

https://doi.org/10.5194/bg-2020-385
Preprint. Discussion started: 10 November 2020

Biogeosciences Discussions Open Access EGU

Table A1. Atmospheric CO_2 measurement sites[a]

Site code	Longitude (degrees)	Latitude (degrees)	Altitude (m)	Site name	U[b] (ppm)
ABP	-38.16	-12.76	6	Arembepe, Bahia	1.04
ALT	-62.51	82.45	195	Alert, Nunavut	1.34
AMY	126.33	36.54	125	Anmyeon-do	8.88
ASC	-14.40	-7.97	90	Ascension Island	0.66
ASK	5.63	23.26	2715	Assekrem	0.80
AZR	-27.08	38.75	24	Terceira Island, Azores	2.26
BAL	16.67	55.50	28	Baltic Sea	5.50
BCS	-110.20	23.30	14	Baja California Sur	3.42
BGU	3.23	41.97	13	Begur	3.93
BHD	174.87	-41.41	90	Baring Head Station	1.12
BKT	100.32	-0.20	875	Bukit Kototabang	3.49
BME	-64.65	32.37	17	St. Davids Head, Bermuda	2.57
BMW	-64.88	32.27	60	Tudor Hill, Bermuda	2.12
BRW	-156.60	71.32	28	Barrow Atmospheric Baseline Observatory	1.88
BSC	28.67	44.18	5	Black Sea, Constanta	9.88
CBA	-162.72	55.20	25	Cold Bay, Alaska	2.41
CFA	147.06	-19.28	5	Cape Ferguson, Queensland	1.04
CGO	144.68	-40.68	164	Cape Grim, Tasmania	0.40
CHR	-157.15	1.70	5	Christmas Island	0.60
CIB	-4.93	41.81	850	Centro de Investigacion de la Baja Atmosfera (CIBA)	3.97
CPT	18.49	-34.35	260	Cape Point	0.74
CRI	73.83	15.08	66	Cape Rama	3.47
CRZ	51.85	-46.43	202	Crozet Island	0.49
CYA	110.52	-66.28	55	Casey, Antarctica	0.29
DRP	-64.91	-55.00	10	Drake Passage	0.41
DSI	116.73	20.70	8	Dongsha Island	3.46
EIC	-109.45	-27.15	55	Easter Island	1.80
ELL	0.96	42.58	2005	Estany Llong	2.41
ESP	-126.53	49.38	47	Estevan Point, British Columbia	1.49
FKL	25.67	35.34	150	Finokalia, Crete	3.34

https://doi.org/10.5194/bg-2020-385
Preprint. Discussion started: 10 November 2020

GMI	144.66	13.39	6	Mariana Islands	2.22
GPA	131.05	-12.25	37	Gunn Point	2.02
HBA	-26.21	-75.61	35	Halley Station, Antarctica	0.16
HPB	11.02	47.80	990	Hohenpeissenberg	6.71
HSU	-124.73	41.05	8	Humboldt State University	5.78
HUN	16.65	46.95	344	Hegyhatsal	6.00
ICE	-20.29	63.40	127	Storhofdi, Vestmannaeyjar	2.03
IZO	-16.48	28.30	2378	Izana, Tenerife, Canary Islands	1.21
KEY	-80.20	25.67	6	Key Biscayne, Florida	4.14
KUM	-154.82	19.52	8	Cape Kumukahi, Hawaii	1.77
KZD	75.57	44.45	412	Sary Taukum	3.19
KZM	77.88	43.25	2524	Plateau Assy	3.00
LJO	-117.26	32.87	20	La Jolla, California	2.72
LLB	-112.45	54.95	546	Lac La Biche, Alberta	8.91
LLN	120.86	23.46	2867	Lulin	5.27
LMP	12.61	35.51	50	Lampedusa	2.08
MAA	62.87	-67.62	42	Mawson Station, Antarctica	0.32
MEX	-97.31	18.98	4469	High Altitude Global Climate Observation Center	1.33
MHD	-9.90	53.33	26	Mace Head, County Galway	3.23
MID	-177.37	28.22	8	Sand Island, Midway	1.39
MKN	37.30	-0.06	3649	Mt. Kenya	1.98
MLO	-155.58	19.53	3402	Mauna Loa, Hawaii	0.63
MQA	158.97	-54.48	13	Macquarie Island	0.33
NAT	-35.26	-5.52	20	Farol De Mae Luiza Lighthouse	1.44
NMB	15.03	-23.58	461	Gobabeb	1.13
NWR	-105.58	40.05	3526	Niwot Ridge, Colorado	1.88
OBN	36.60	55.12	484	Obninsk	6.49
OTA	142.82	-38.52	50	Otway, Victoria	17.45
OXK	11.81	50.03	1185	Ochsenkopf	8.18
PAL	24.12	67.97	570	Pallas-Sammaltunturi, GAW Station	3.72
PDM	0.14	42.94	2877	Pic Du Midi	2.71
POC	-145.13	14.97	20	Pacific Ocean	1.47
PSA	-64.00	-64.92	15	Palmer Station, Antarctica	0.23

https://doi.org/10.5194/bg-2020-385
Preprint. Discussion started: 10 November 2020

PTA	-123.73	38.95	22	Point Arena, California	5.50
RK1	-177.90	-29.20	12	Kermadec Island	2.23
RPB	-59.43	13.17	20	Ragged Point	0.83
SDZ	117.12	40.65	298	Shangdianzi	9.57
SEY	55.53	-4.68	7	Mahe Island, Seychelles	0.98
SGP	-97.48	36.62	374	Southern Great Plains, Oklahoma	4.91
SHM	174.10	52.72	28	Shemya Island, Alaska	2.91
SIS	-1.26	60.09	33	Shetland Islands	2.87
SMO	-170.57	-14.25	47	Tutuila, American Samoa	1.19
STM	2.00	66.00	7	Ocean Station M	2.03
SUM	-38.42	72.60	3215	Summit	1.32
SYO	39.58	-69.00	16	Syowa Station, Antarctica	0.23
TAC	1.14	52.52	236	Tacolneston	6.78
TAP	126.13	36.73	21	Tae-ahn Peninsula	6.90
THD	-124.15	41.05	112	Trinidad Head, California	4.54
TIK	128.89	71.60	29	Hydrometeorological Observatory of Tiksi	2.64
USH	-68.31	-54.85	32	Ushuaia	1.41
UTA	-113.72	39.90	1332	Wendover, Utah	2.65
UUM	111.10	44.45	1012	Ulaan Uul	2.78
WIS	34.78	30.86	482	Weizmann Institute of Science at the Arava Institute, Ketura	2.39
WLG	100.92	36.27	3815	Mt. Waliguan	2.26
WPC	167.50	-29.86	10	Western Pacific Cruise	1.70
ZEP	11.89	78.91	479	Ny-Alesund, Svalbard	1.82

[a] Source reference: Cooperative Global Atmospheric Data Integration Project, 2018. Version: obspack_co2_1_GLOBALVIEWplus_v4.2_2019-03-19 (https://doi.org/10.25925/20190319)

[b] The specification of observational uncertainty U on atmospheric CO_2 measurements (and represented in matrix *R* of Equation A1) is calculated as the standard deviation of measurement variability and using the detrended and deseasonalized CO_2 time series at each measurement site (following methods of Chevallier et al. (2010)).

Data Availability. Data sources: (i) Atmospheric CO_2 measurements were taken from obspack_co2_1_GLOBALVIEWplus_v4.2_2019-03-19 (https://doi.org/10.25925/20190319); (ii) Prior ocean flux oc_v1.7 from Rödenbeck et al . (2013) taken from http://www.bgc-jena.mpg.de/CarboScope/. Prior ocean flux Landschützer et al. (2016) taken from https://www.nodc.noaa.gov/ocads/oceans/SPCO2_1982_present_ETH_SOM_FFN.html. Prior ocean flux

https://doi.org/10.5194/bg-2020-385
Preprint. Discussion started: 10 November 2020

from Takahashi et al. (2009) taken from ftp://ftp.as.harvard.edu/gcgrid/geos-chem. (iii) CarbonTracker CT2019 results provided by NOAA ESRL, Boulder, Colorado, USA from the website at http://carbontracker.noaa.gov. CTE flux estimates taken from ftp://ftp.wur.nl/carbontracker/data/fluxes/data_flux1x1_monthly/. The flux estimates from CAMS(v18r2) taken from https://apps.ecmwf.int/datasets/data/cams-ghg-inversions/. (iv) The model CO_2 fluxes for JULES (land) and GOBMs (ocean) taken from (Le Quéré et al., 2018).

Author contributions. ZC and PS designed the study. ZC, PS, JZ and NZ developed the model. ZC, PS, AW, and US discussed the design of simulations. ZC performed the simulations and analysis and wrote the initial manuscript. All authors contributed to the writing of the paper.

Competing interests. The authors declare that they have no conflict of interest.

Disclaimer. The work reflects only the author's view,the Europen Commission and their executive agency are not responsible for any use that may be made of the information the work contains.

Acknowledgements. This work was performed using the High Performance Computing Cluster at the University of East Anglia.

Financial support. It was supported through the UK Natural Environment Research Council grants NE/K002473/1(RAGNARoCC).

References

Bopp, L., Resplandy, L., Orr, J. C., Doney, S. C., Dunne, J. P., Gehlen, M., Halloran, P., Heinze, C., Ilyina, T., and Seferian, R.: Multiple stressors of ocean ecosystems in the 21st century: projections with CMIP5 models, Biogeosciences, 10, 6225-6245, https://doi.org/10.5194/bg-10-6225-2013, 2013.

Buitenhuis, E. T., Rivkin, R. B., Sailley, S., and Le Quéré, C.: Biogeochemical fluxes through microzooplankton, Global Biogeochemical Cycles, 24, GB4015, https://doi.org/10.1029/2009GB003601, 2010.

Carouge, C., Bousquet, P., Peylin, P., Rayner, P., and Ciais, P.: What can we learn from European continuous atmospheric CO_2 measurements to quantify regional fluxes--Part 1: Potential of the 2001 network, Atmospheric Chemistry & Physics, 10, 3107-3117, https://doi.org/10.5194/acp-10-3107-2010, 2010.

Chatterjee, A., Engelen, R. J., Kawa, S. R., Sweeney, C., and Michalak, A. M.: Background error covariance estimation for atmospheric CO_2 data assimilation, Journal of Geophysical Research: Atmospheres, 118, 10140-10154, https://doi.org/10.1002/jgrd.50564, 2013.

Chevallier, F., Ciais, P., Conway, T., Aalto, T., Anderson, B., Bousquet, P., Brunke, E., Ciattaglia, L., Esaki, Y., and Fröhlich, M.: CO_2 surface fluxes at grid point scale estimated from a global 21 year reanalysis of atmospheric measurements, Journal of

https://doi.org/10.5194/bg-2020-385
Preprint. Discussion started: 10 November 2020

390 Geophysical Research: Atmospheres, 115, D21307, https://doi.org/10.1029/2010JD013887, 2010.

Chevallier, F., Palmer, P. I., Feng, L., Boesch, H., O'Dell, C. W., and Bousquet, P.: Toward robust and consistent regional CO_2 flux estimates from in situ and spaceborne measurements of atmospheric CO_2, Geophysical Research Letters, 41, 1065-1070, https://doi.org/10.1002/2013GL058772, 2014.

Chevallier, F., Remaud, M., O'Dell, C. W., Baker, D., Peylin, P., and Cozic, A.: Objective evaluation of surface-and satellite-
395 driven carbon dioxide atmospheric inversions, Atmospheric Chemistry and Physics, 19, 14233-14251, https://doi.org/10.5194/acp-19-14233-2019, 2019.

Clark, D., Mercado, L., Sitch, S., Jones, C., Gedney, N., Best, M., Pryor, M., Rooney, G., Essery, R., Blyth, E., Boucher, O., Harding, R., Huntingford, C., and Cox, P.: The Joint UK Land Environment Simulator (JULES), model description - Part 2: Carbon fluxes and vegetation dynamics, Geoscientific Model Development, 4, 701-722, https://doi.org/10.5194/gmd-4-701-
400 2011, 2011.

Crippa, M., Janssens-Maenhout, G., Dentener, F., Guizzardi, D., Sindelarova, K., Muntean, M., Van Dingenen, R., and Granier, C.: Forty years of improvements in European air quality: regional policy-industry interactions with global impacts, Atmospheric Chemistry and Physics, 16, 3825-3841, https://doi.org/10.5194/acp-16-3825-2016, 2016.

Deng, F., Jones, D. B. A., Parazoo, N. C., O'Dell, C. W., and Nassar, R.: Combining GOSAT XCO_2 observations over land
405 and ocean to improve regional CO_2 flux estimates, Journal of Geophysical Research: Atmospheres, 121, 1896-1913, https://doi.org/10.1002/2015JD024157, 2016.

DeVries, T., Le Quéré, C., Andrews, O., Berthet, S., Hauck, J., Ilyina, T., Landschützer, P., Lenton, A., Lima, I. D., and Nowicki, M.: Decadal trends in the ocean carbon sink, Proceedings of the National Academy of Sciences, 116, 11646-11651, https://doi.org/10.1073/pnas.1900371116, 2019.

410 Doney, S. C., Lima, I., Feely, R. A., Glover, D. M., Lindsay, K., Mahowald, N., Moore, J. K., and Wanninkhof, R.: Mechanisms governing interannual variability in upper-ocean inorganic carbon system and air–sea CO_2 fluxes: Physical climate and atmospheric dust, Deep Sea Research Part II: Topical Studies in Oceanography, 56, 640-655, https://doi.org/10.1016/j.dsr2.2008.12.006, 2009.

Feng, L., Palmer, P., Bösch, H., and Dance, S.: Estimating surface CO_2 fluxes from space-borne CO_2 dry air mole fraction
415 observations using an ensemble Kalman Filter, Atmospheric Chemistry & Physics, 9, 2619-2633, https://doi.org/10.5194/acp-9-2619-2009, 2009.

Feng, L., Palmer, P. I., Parker, R. J., Deutscher, N. M., Feist, D., Kivi, R., Morino, I., and Sussmann, R.: Estimates of European uptake of CO_2 inferred from GOSAT XCO_2 retrievals: sensitivity to measurement bias inside and outside Europe, Atmospheric Chemistry and Physics, 16, 1289-1302, https://doi.org/10.5194/acp-16-1289-2016, 2016.

420 Friedlingstein, P., Jones, M. W., O'Sullivan, M., Andrew, R. M., Hauck, J., Peters, G. P., Peters, W., Pongratz, J., Sitch, S., Le Quéré, C., Bakker, D. C. E., Canadell, J. G., Ciais, P., Jackson, R. B., Anthoni, P., Barbero, L., Bastos, A., Bastrikov, V., Becker, M., Bopp, L., Buitenhuis, E., Chandra, N., Chevallier, F., Chini, L. P., Currie, K. I., Feely, R. A., Gehlen, M., Gilfillan, D., Gkritzalis, T., Goll, D. S., Gruber, N., Gutekunst, S., Harris, I., Haverd, V., Houghton, R. A., Hurtt, G., Ilyina, T., Jain, A.

https://doi.org/10.5194/bg-2020-385
Preprint. Discussion started: 10 November 2020

K., Joetzjer, E., Kaplan, J. O., Kato, E., Goldewijk, K. K., Korsbakken, J. I., Landschützer, P., Lauvset, S. K., Lefèvre, N., Lenton, A., Lienert, S., Lombardozzi, D., Marland, G., McGuire, P. C., Melton, J. R., Metzl, N., Munro, D. R., Nabel, J. E. M. S., Nakaoka, S. I., Neill, C., Omar, A. M., Ono, T., Peregon, A., Pierrot, D., Poulter, B., Rehder, G., Resplandy, L., Robertson, E., Rödenbeck, C., Séférian, R., Schwinger, J., Smith, N., Tans, P. P., Tian, H. Q., Tilbrook, B., Tubiello, F. N., van der Werf, G. R., Wiltshire, A. J., and Zaehle, S.: Global Carbon Budget 2019, Earth System Science Data, 11, 1783-1838, https://doi.org/10.5194/essd-11-1783-2019, 2019.

Gaubert, B., Stephens, B. B., Basu, S., Chevallier, F., Deng, F., Kort, E. A., Patra, P. K., Peters, W., Rödenbeck, C., and Saeki, T.: Global atmospheric CO_2 inverse models converging on neutral tropical land exchange, but disagreeing on fossil fuel and atmospheric growth rate, Biogeosciences, 16, 117-134, https://doi.org/10.5194/bg-16-117-2019, 2019.

Gruber, N., Gloor, M., Mikaloff Fletcher, S. E., Doney, S. C., Dutkiewicz, S., Follows, M. J., Gerber, M., Jacobson, A. R., Joos, F., and Lindsay, K.: Oceanic sources, sinks, and transport of atmospheric CO_2, Global Biogeochemical Cycles, 23, GB1005, https://doi.org/10.1029/2008GB003349, 2009.

Gruber, N., Landschützer, P., and Lovenduski, N. S.: The variable Southern Ocean carbon sink, Annual Review of Marine Science, 11, 159-186, https://doi.org/10.1146/annurev-marine-121916-063407, 2019.

Gurney, K. R., Law, R. M., Denning, A. S., Rayner, P. J., Baker, D., Bousquet, P., Bruhwiler, L., Chen, Y. H., Ciais, P., and Fan, S.: TransCom 3 CO_2 inversion intercomparison: 1. Annual mean control results and sensitivity to transport and prior flux information, Tellus B: Chemical and Physical Meteorology, 55B, 555-579, https://doi.org/10.3402/tellusb.v55i2.16728, 2003.

Hauck, J., Köhler, P., Wolf-Gladrow, D., and Völker, C.: Iron fertilisation and century-scale effects of open ocean dissolution of olivine in a simulated CO_2 removal experiment, Environmental Research Letters, 11, 024007, https://doi.org/10.1088/1748-9326/11/2/024007, 2016.

Hunt, B. R., Kostelich, E. J., and Szunyogh, I.: Efficient data assimilation for spatiotemporal chaos: A local ensemble transform Kalman filter, Physica D: Nonlinear Phenomena, 230, 112-126, https://doi.org/10.1016/j.physd.2006.11.008, 2007.

Ilyina, T., Six, K. D., Segschneider, J., Maier-Reimer, E., Li, H., and Núñez-Riboni, I.: Global ocean biogeochemistry model HAMOCC: Model architecture and performance as component of the MPI-Earth system model in different CMIP5 experimental realizations, Journal of Advances in Modeling Earth Systems, 5, 287-315, https://doi.org/10.1029/2012MS000178, 2013.

Jacobson, A. R., Mikaloff Fletcher, S. E., Gruber, N., Sarmiento, J. L., and Gloor, M.: A joint atmosphere-ocean inversion for surface fluxes of carbon dioxide: 1. Methods and global-scale fluxes, Global Biogeochemical Cycles, 21, GB1019, https://doi.org/10.1029/2005GB002556, 2007.

Jacobson, A. R., Schuldt, K. N., Miller, J. B., Oda, T., Tans, P., Andrews, A., Mund, J., Ott, L., Collatz, G. J., Aalto, T., Afshar, S., Aikin, K., Aoki, S., Apadula, F., Baier, B., Bergamaschi, P., Beyersdorf, A., Biraud, S. C., Bollenbacher, A., Bowling, D., Brailsford, G., Abshire, J. B., Chen, G., Chen, H., Chmura, L., Climadat, S., Colomb, A., Conil, S., Cox, A., Cristofanelli, P., Cuevas, E., Curcoll, R., Sloop, C. D., Davis, K., Wekker, S. D., Delmotte, M., DiGangi, J. P., Dlugokencky, E., Ehleringer, J., Elkins, J. W., Emmenegger, L., Fischer, M. L., Forster, G., Frumau, A., Galkowski, M., Gatti, L. V., Gloor, E., Griffis, T.,

https://doi.org/10.5194/bg-2020-385
Preprint. Discussion started: 10 November 2020

Hammer, S., Haszpra, L., Hatakka, J., Heliasz, M., Hensen, A., Hermanssen, O., Hintsa, E., Holst, J., Jaffe, D., Karion, A., Kawa, S. R., Keeling, R., Keronen, P., Kolari, P., Kominkova, K., Kort, E., Krummel, P., Kubistin, D., Labuschagne, C., Langenfelds, R., Laurent, O., Laurila, T., Lauvaux, T., Law, B., Lee, J., Lehner, I., Leuenberger, M., Levin, I., Levula, J., Lin, J., Lindauer, M., Loh, Z., Lopez, M., Lund Myhre, C., Machida, T., Mammarella, I., Manca, G., Manning, A., Manning, A., Marek, M. V., Marklund, P., Martin, M. Y., Matsueda, H., McKain, K., Meijer, H., Meinhardt, F., Miles, N., Miller, C. E., Mölder, M., Montzka, S., Moore, F., Morgui, J., Morimoto, S., Munger, B., Necki, J., ¨Newman, S., Nichol, S., Niwa, Y., O'Doherty, S., Ottosson-Löfvenius, M., Paplawsky, B., Peischl, J., Peltola, O., Pichon, J., Piper, S., Plass-Dölmer, C., Ramonet, M., Reyes-Sanchez, E., Richardson, S., Riris, H., Ryerson, T., Saito, K., Sargent, M., Sasakawa, M., Sawa, Y., Say, D., Scheeren, B., Schmidt, M., Schmidt, A., Schumacher, M., Shepson, P., Shook, M., Stanley, K., Steinbacher, M., Stephens, B., Sweeney, C., Thoning, K., Torn, M., Turnbull, J., Tørseth, K., van den Bulk, P., van der Laan−Luijkx, I. T., van Dinther, D., Vermeulen, A., Viner, B., Vitkova, G., Walker, S., Weyrauch, D., Wofsy, S., Worthy, D., Young, D., and Zimnoch, M., CarbonTracker CT2019, Model published by NOAA Earth System Research Laboratory, Global Monitoring Division, https://doi.org/ 10.25925/39m3-6069, 2020.

Kang, J. S., Kalnay, E., Miyoshi, T., Liu, J., and Fung, I.: Estimation of surface carbon fluxes with an advanced data assimilation methodology, Journal of Geophysical Research: Atmospheres, 117, D24101, https://doi.org/10.1029/2012JD018259, 2012.

Khatiwala, S. P., Tanhua, T., Mikaloff Fletcher, S. E., Gerber, M., Doney, S. C., Graven, H. D., Gruber, N., McKinley, G., Murata, A., and Ríos, A.: Global ocean storage of anthropogenic carbon, Biogeosciences, 10, 2169-2191, https://doi.org/10.5194/bg-10-2169-2013, 2013.

Landschuetzer, P., Gruber, N., and Bakker, D. C.: Decadal variations and trends of the global ocean carbon sink, Global Biogeochemical Cycles, 30, 1396-1417, https://doi.org/10.1002/2015GB005359, 2016.

Landschützer, P., Gruber, N., Bakker, D. C., Schuster, U., Nakaoka, S. I., Payne, M. R., Sasse, T. P., and Zeng, J.: A neural network-based estimate of the seasonal to inter-annual variability of the Atlantic Ocean carbon sink, Biogeosciences, 10, 7793-7815, https://doi.org/10.5194/bg-10-7793-2013, 2013.

Landschützer, P., Ilyina, T., and Lovenduski, N. S.: Detecting Regional Modes of Variability in Observation-Based Surface Ocean pCO_2, Geophysical Research Letters, 46, 2670-2679, https://doi.org/10.1029/2018GL081756, 2019.

Law, R. M., Ziehn, T., Matear, R. J., Lenton, A., Chamberlain, M. A., Stevens, L. E., Ying-Ping, W., Srbinovsky, J., Bi, D., and Yan, H.: The carbon cycle in the Australian Community Climate and Earth System Simulator (ACCESS-ESM1)–Part 1: Model description and pre-industrial simulation, Geoscientific Model Development, 10, 2567-2590, https://doi.org/10.6194/gmd-10-2567-2017, 2017.

Le Quéré, C., Andrew, R. M., Friedlingstein, P., Sitch, S., Pongratz, J., Manning, A. C., Korsbakken, J. I., Peters, G. P., Canadell, J. G., Jackson, R. B., Boden, T. A., Tans, P. P., Andrews, O. D., Arora, V. K., Bakker, D. C. E., Barbero, L., Becker, M., Betts, R. A., Bopp, L., Chevallier, F., Chini, L. P., Ciais, P., Cosca, C. E., Cross, J., Currie, K., Gasser, T., Harris, I., Hauck, J., Haverd, V., Houghton, R. A., Hunt, C. W., Hurtt, G., Ilyina, T., Jain, A. K., Kato, E., Kautz, M., Keeling, R. F.,

https://doi.org/10.5194/bg-2020-385
Preprint. Discussion started: 10 November 2020

Klein Goldewijk, K., Körtzinger, A., Landschützer, P., Lefèvre, N., Lenton, A., Lienert, S., Lima, I., Lombardozzi, D., Metzl, N., Millero, F., Monteiro, P. M. S., Munro, D. R., Nabel, J. E. M. S., Nakaoka, S., Nojiri, Y., Padin, X. A., Peregon, A., Pfeil, B., Pierrot, D., Poulter, B., Rehder, G., Reimer, J., Rödenbeck, C., Schwinger, J., Séférian, R., Skjelvan, I., Stocker, B. D., Tian, H., Tilbrook, B., Tubiello, F. N., van der Laan−Luijkx, I. T., van der Werf, G. R., van Heuven, S., Viovy, N., Vuichard, N., Walker, A. P., Watson, A. J., Wiltshire, A. J., Zaehle, S., and Zhu, D.: Global carbon budget 2017, Earth System Science Data, 10, 405-448, https://doi.org/10.5194/essd-10-405-2018, 2018.

Lebehot, A. D., Halloran, P. R., Watson, A. J., McNeall, D., Ford, D. A., Landschützer, P., Lauvset, S. K., and Schuster, U.: Reconciling observation and model trends in North Atlantic surface CO_2, Global Biogeochemical Cycles, 33, 1204-1222, https://doi.org/10.1029/2019GB006186, 2019.

Liu, J., Bowman, K. W., and Henze, D. K.: Source-receptor relationships of column-average CO_2 and implications for the impact of observations on flux inversions, Journal of Geophysical Research: Atmospheres, 120, 5214-5236, https://doi.org/10.1002/2014JD022914, 2015.

Liu, J., Bowman, K. W., and Lee, M.: Comparison between the Local Ensemble Transform Kalman Filter (LETKF) and 4D-Var in atmospheric CO_2 flux inversion with the Goddard Earth Observing System-Chem model and the observation impact diagnostics from the LETKF, Journal of Geophysical Research: Atmospheres, 121, 13,066-013,087, https://doi.org/10.1002/2016JD025100, 2016.

Liu, Y., Kalnay, E., Zeng, N., Asrar, G., Chen, Z., and Jia, B.: Estimating surface carbon fluxes based on a local ensemble transform Kalman filter with a short assimilation window and a long observation window: an observing system simulation experiment test in GEOS-Chem 10.1, Geoscientific Model Development, 12, 2899-2914, https://doi.org/10.5194/gmd-12-2899-2019, 2019.

Macovei, V. A., Hartman, S. E., Schuster, U., Torres-Valdés, S., Moore, C. M., and Sanders, R. J.: Impact of physical and biological processes on temporal variations of the ocean carbon sink in the mid-latitude North Atlantic (2002–2016), Progress in Oceanography, 180, 102223, https://doi.org/10.1016/j.pocean.2019.102223, 2020.

McKinley, G. A., Fay, A. R., Takahashi, T., and Metzl, N.: Convergence of atmospheric and North Atlantic carbon dioxide trends on multidecadal timescales, Nature Geoscience, 4, 606-610, https://doi.org/10.1038/ngeo1193, 2011.

Mikaloff Fletcher, S., Gruber, N., Jacobson, A. R., Doney, S., Dutkiewicz, S., Gerber, M., Follows, M., Joos, F., Lindsay, K., and Menemenlis, D.: Inverse estimates of anthropogenic CO_2 uptake, transport, and storage by the ocean, Global Biogeochemical Cycles, 20, GB2002, https://doi.org/10.1029/2005GB002530, 2006.

Miyoshi, T., Yamane, S., and Enomoto, T.: Localizing the error covariance by physical distances within a local ensemble transform Kalman filter (LETKF), SOLA, 3, 089-092, https://doi.org/10.2151/sola.2007-023, 2007.

Montgomery, D. C., Peck, E. A., and Vining, G. G.: Introduction to Linear Regression Analysis,5th Edition, John Wiley & Sons, 2012.

Nassar, R., Jones, D. B., Suntharalingam, P., Chen, J. M., Andres, R. J., Wecht, K. J., Yantosca, R. M., Kulawik, S. S., Bowman, K. W., and Worden, J. R.: Modeling global atmospheric CO_2 with improved emission inventories and CO_2

https://doi.org/10.5194/bg-2020-385
Preprint. Discussion started: 10 November 2020

production from the oxidation of other carbon species, Geoscientific Model Development, 3, 689-716, https://doi.org/10.5194/gmd-3-689-2010, 2010.

Nassar, R., Jones, D. B. A., Kulawik, S. S., Worden, J. R., Bowman, K. W., Andres, R. J., Suntharalingam, P., Chen, J. M., Brenninkmeijer, C., and Schuck, T.: Inverse modeling of CO_2 sources and sinks using satellite observations of CO_2 from TES and surface flask measurements, Atmospheric Chemistry and Physics, 11, 6029-6047, https://doi.org/10.5194/acp-11-6029-2011, 2011.

Peters, W., Miller, J., Whitaker, J., Denning, A., Hirsch, A., Krol, M., Zupanski, D., Bruhwiler, L., and Tans, P.: An ensemble data assimilation system to estimate CO_2 surface fluxes from atmospheric trace gas observations, Journal of Geophysical Research: Atmospheres, 110, D24304, https://doi.org/10.1029/2005JD006157, 2005.

Peylin, P., Law, R., Gurney, K., Chevallier, F., Jacobson, A., Maki, T., Niwa, Y., Patra, P., Peters, W., and Rayner, P.: Global atmospheric carbon budget: results from an ensemble of atmospheric CO_2 inversions, Biogeosciences, 10, 6699-6720, https://doi.org/10.5194/bg-10-6699-2013, 2013.

Rienecker, M. M., Suarez, M., Todling, R., Bacmeister, J., Takacs, L., Liu, H., Gu, W., Sienkiewicz, M., Koster, R., and Gelaro, R.: The GEOS-5 Data Assimilation System: Documentation of Versions 5.0. 1, 5.1. 0, and 5.2. 0, NASA Technical Report Series on Global Modelling and Data Assimilation,NASA/TM–2008–104606, 27, 2008.

Rödenbeck, C., Houweling, S., Gloor, M., and Heimann, M.: Time-dependent atmospheric CO_2 inversions based on interannually varying tracer transport, Tellus, 55B, 488-497, https://doi.org/10.3402/tellusb.v55i2.16707, 2003.

Rödenbeck , C., Bakker, D. C. E., Metzl, N., Olsen, A., Sabine, C., Reum, F., Keeling, R. F., and Heimann, M.: Interannual sea-air CO_2 flux variability from an observation-driven ocean mixed-layer scheme, Biogeosciences, 11, 4599-4613, https://doi.org/10.5194/bg-11-4599-2014, 2014.

Rödenbeck, C., Bakker, D. C., Gruber, N., Iida, Y., Jacobson, A. R., Jones, S., Landschützer, P., Metzl, N., Nakaoka, S., and Olsen, A.: Data-based estimates of the ocean carbon sink variability–first results of the Surface Ocean pCO_2 Mapping intercomparison (SOCOM), Biogeosciences, 12, 7251-7278, https://doi.org/10.5194/bg-12-7251-2015, 2015.

Sabine, C. L., Feely, R. A., Gruber, N., Key, R. M., Lee, K., Bullister, J. L., Wanninkhof, R., Wong, C., Wallace, D. W., and Tilbrook, B.: The oceanic sink for anthropogenic CO_2, Science, 305, 367-371, https://doi.org/10.1126/science.1097403, 2004.

Schuster, U., McKinley, G. A., Bates, N., Chevallier, F., Doney, S. C., Fay, A., González-Dávila, M., Gruber, N., Jones, S., and Krijnen, J.: An assessment of the Atlantic and Arctic sea-air CO_2 fluxes, 1990-2009, Biogeosciences, 10, 607-627, https://doi.org/10.5194/bg-10-607-2013, 2013.

Schwinger, J., Goris, N., Tjiputra, J. F., Kriest, I., Bentsen, M., Bethke, I., Ilicak, M., Assmann, K. M., and Heinze, C.: Evaluation of NorESM-OC (versions 1 and 1.2), the ocean carbon-cycle stand-alone configuration of the Norwegian Earth System Model (NorESM1), Geoscientific Model Development, 9, 2589-2622, https://doi.org/10.5194/gmd-9-2589-2016, 2016.

Suntharalingam, P., Randerson, J. T., Krakauer, N., Logan, J. A., and Jacob, D. J.: Influence of reduced carbon emissions and oxidation on the distribution of atmospheric CO_2: Implications for inversion analyses, Global Biogeochemical Cycles, 19,

560 GB4003, https://doi.org/10.1029/2005GB002466, 2005.

Séférian, R., Bopp, L., Gehlen, M., Orr, J. C., Ethé, C., Cadule, P., Aumont, O., y Mélia, D. S., Voldoire, A., and Madec, G.: Skill assessment of three earth system models with common marine biogeochemistry, Climate Dynamics, 40, 2549-2573, https://doi.org/10.1007/s00382-012-1362-8, 2013.

Takahashi, T., Sutherland, S. C., Sweeney, C., Poisson, A., Metzl, N., Tilbrook, B., Bates, N., Wanninkhof, R., Feely, R. A.,
565 and Sabine, C.: Global sea–air CO_2 flux based on climatological surface ocean pCO_2, and seasonal biological and temperature effects, Deep Sea Research Part II: Topical Studies in Oceanography, 49, 1601-1622, https://doi.org/10.1016/S0967-0645(02)00003-6, 2002.

Takahashi, T., Sutherland, S. C., Wanninkhof, R., Sweeney, C., Feely, R. A., Chipman, D. W., Hales, B., Friederich, G., Chavez, F., and Sabine, C.: Climatological mean and decadal change in surface ocean pCO_2, and net sea–air CO_2 flux over the
570 global oceans, Deep Sea Research Part II: Topical Studies in Oceanography, 56, 554-577, https://doi.org/10.1016/j.dsr2.2008.12.009, 2009.

Van Der Laan−Luijkx, I. T., Van Der Velde, I. R., Van Der Veen, E., Tsuruta, A., Stanislawska, K., Babenhauserheide, A., Zhang, H. F., Liu, Y.-N., He, W., and Chen, H.: The CarbonTracker Data Assimilation Shell (CTDAS) v1. 0: implementation and global carbon balance 2001-2015, Geoscientific Model Development, 10, 2785-2800, https://doi.org/10.5194/gmd-10-
575 2785-2017, 2017.

Wanninkhof, R., Pickers, P., Omar, A., Sutton, A., Murata, A., Olsen, A., Bb, S., Tilbrook, B., Munro, D., and Pierrot, D.: A surface ocean CO_2 reference network, SOCONET and associated marine boundary layer CO_2 measurements, Frontiers in Marine Science, 6, https://doi.org/10.3389/fmars.2019.00400, 2019.

Watson, A. J., Schuster, U., Bakker, D. C., Bates, N. R., Corbière, A., González-Dávila, M., Friedrich, T., Hauck, J., Heinze,
580 C., and Johannessen, T.: Tracking the variable North Atlantic sink for atmospheric CO_2, Science, 326, 1391-1393, https://doi.org/10.1126/science.1177394, 2009.